The Astrophysical Journal, 904:7 (7pp), 2020 November 20 https://doi.org/10.3847/1538-4357/abbb36

Magnetic Energy Balance in the Quiet Sun on Supergranular Spatial and Temporal Scales

Fabio Giannattasio[1], Giuseppe Consolini[2], Francesco Berrilli[3], and Dario Del Moro[3]
[1] Istituto Nazionale di Geofisica e Vulcanologia, Via di Vigna Murata 605, I-00143 Roma, Italy; fabio.giannattasio@ingv.it
[2] INAF—Istituto di Astrofisica e Planetologia Spaziali, Via del Fosso del Cavaliere 100, I-00133 Roma, Italy
[3] Department of Physics, University of Rome Tor Vergata, Via della Ricerca Scientifica 1, I-00133 Roma, Italy
Received 2020 June 29; revised 2020 August 30; accepted 2020 September 17; published 2020 November 17

Abstract

Small-scale magnetic fields are ubiquitous in the quiet solar photosphere and may store and transfer huge amounts of energy to the upper atmospheric layers. For this reason, it is fundamental to constrain the energetics of the quiet Sun. By taking advantage of a 24 hr long magnetogram time series acquired by the Hinode mission without interruption, we computed, for the first time, the average rate of change of magnetic energy density on supergranular spatial and temporal scales. We found that the regions where this quantity is positive correspond with the longest magnetic field decorrelation times, with the latter being consistent with the timescales of magnetic energy density variation. This suggests that, on average, the energy provided by photospheric electric and magnetic fields and current density is effective in sustaining the magnetic fields in the network.

Unified Astronomy Thesaurus concepts: Solar photosphere (1518); Supergranulation (1662); Quiet sun (1322); Solar magnetic fields (1503); Space weather (2037)

1. Introduction

The study of the mechanisms responsible for the storage of energy in the solar photosphere and its transport to the upper atmospheric layers is of uttermost importance in active regions as well as in the quiet Sun, where they may trigger a chain of phenomena relevant for space weather. In this framework, a substantial contribution to the energy budget of the photosphere is carried by ubiquitous small-scale magnetic fields (magnetic elements, MEs) with characteristic size of the order of—and smaller than—the spatial resolution (about 100 km) achievable by current instruments (see, e.g., Trujillo Bueno et al. 2004; Bellot Rubio & Orozco Suárez 2019). Several studies in the literature have pointed out the key role played by MEs in storing energy in the quiet Sun and their capability to transfer it upward via, for instance, magnetic reconnections (see, e.g., Chae 1999; Viticchié et al. 2006; Rouppe van der Voort et al. 2016; Gošić et al. 2018; Bellot Rubio & Orozco Suárez 2019, and references therein) and/or magnetohydrodynamic waves (see, e.g., Hahn & Savin 2014; Stangalini et al. 2015; Jefferies et al. 2019; Rajaguru et al. 2019, and references therein). However, the processes by which MEs emerge, evolve, and organize in the quiet photosphere are still not completely clear, despite the recent efforts aimed to characterize their dynamics on a wide range of spatial and temporal scales, from granular to supergranular (see, e.g., Giannattasio et al. 2013, 2014b, 2014a; Abramenko 2017; Giannattasio et al. 2018; Bellot Rubio & Orozco Suárez 2019; Giannattasio et al. 2019, and references therein).

In order to correctly estimate the amount of available energy in a given photospheric region it is necessary to know the electric field, $\boldsymbol{E}$, and the current density, $\boldsymbol{J}$, as well as the magnetic field, $\boldsymbol{B}$. In fact, all these quantities allow us to compute, for example, the Poynting flux, the magnetic helicity (see, e.g., Démoulin & Berger 2003; Schuck 2006; Kazachenko et al. 2014, 2015) and study the evolution of currents and their coupling with electric and magnetic fields. In particular, the variation of the magnetic energy content in a volume of photospheric plasma is linked to the work done by the field forces on a distribution of charges via the Poynting' s theorem, which states that the rate of variation of the energy density equals the work done by the electric field plus the net rate of energy flux escaping the plasma volume element. More in detail, the rate of work done on the surrounding plasma is expressed via the dot product, $\boldsymbol{J}\cdot\boldsymbol{E}$, while the energy flux is described by the divergence of the Poynting vector, $\boldsymbol{S}$. Thus, the interaction between $\boldsymbol{E}$, $\boldsymbol{J}$, and $\boldsymbol{B}$ plays a fundamental role in the energy balance of the photospheric plasma.

While the computation of the current density does not present criticalities once provided the vector magnetic field, and can be attained by invoking the Ampere's law, the computation of electric field is not trivial and has some aspects to pay attention to. Mainly two techniques have been used in the past to compute the electric field: the spectroscopy observation of the Stark effect (Wien 1916; Davis 1977; Jordan et al. 1980) and the use of the Ohms law in the ideal MHD regime. While the former method was recognized to be critically affected by the low sensitivity of observations (Moran & Foukal 1991); the latter was improved by considering the component of the Faradays equation orthogonal to the magnetic field so to obtain both velocity and electric field vectors (Kusano et al. 2002; Welsch et al. 2004; Chae & Sakurai 2008). Various refined techniques have been developed to compute the electric field based on the Faradays law mixed with observational constraints (see, e.g., Fisher et al. 2010; Kazachenko et al. 2014). These methods are as accurate as they are complex, and require input vector magnetograms or full-Stokes data to perform spectropolarimetric inversions via suitable numerical procedures. These requirements imply the acceptance of trade-offs in observations, as it is at present still not possible to take advantage of robust vector magnetograms (or full-Stokes data to be successfully inverted) at very high spatial resolution and at the same time cover a wide range of both spatial and temporal scales (from granular to at least supergranular scales). However, when dealing with observations targeted at the quiet Sun a reasonable approximation for

the photospheric electric field can still be obtained also having only line-of-sight (LoS) magnetograms instead of full vector magnetograms as inputs when averaging over the longest timescales available (let us say of the order of typical timescale of supergranulation). In this case the computation of electric field is much simplified while, in contrast, none of the accurate methods mentioned above are applicable to compute such an averaged photospheric electric field on supergranular scales.

As far as we know, the average properties of photospheric electric field and current density in the quiet Sun on supergranular spatial and temporal scales still have not been, or have been poorly, investigated, although they may play a crucial role in the storage and dissipation of energy in the quiet photosphere. In this work, for the first time we provide an average description of the properties of both the photospheric electric field and current density in the quiet Sun on supergranular scales and their connection with the magnetic energy budget of the photosphere. We take advantage of an unprecedented data set consisting of a ∼24 hr long magnetogram time series with high spatial resolution (≃0.″3) targeted at the disk center and enclosing an entire supergranule, whose linear size is about ∼50″. The results obtained are discussed in the light of recent studies in the literature and may help to shed light on the mechanisms that cause the variation of magnetic energy in the quiet photosphere. The paper is organized as follows. In Section 2 we describe the data set used and the approach by which the physical quantities averaged on supergranular scales are computed. Section 3 is devoted to the description of results and their discussion in the light of the previous literature; while in Section 4 we summarize our findings and draw conclusions.

2. Data and Methods

2.1. The Data Set

The data analyzed in this work were acquired by the Hinode mission (Kosugi et al. 2007) on 2010 November 2, and are part of the Hinode Operation Plan 151 entitled "Flux replacement in the photospheric network and internetwork." They consist of a magnetogram times series with 90 s cadence starting at 08:00:42 UT, lasting for ∼24 hr without interruption, and targeted at a quiet Sun region in the disk center. Magnetograms were produced by using the spectral line Na I D at 589.6 nm, observed with the Narrowband Filter Imager (Tsuneta et al. 2008) at two wavelengths at ±160 mÅ from the line center. Data were 2 × 2 binned to a pixel size of 0.″16, corresponding to ≃116 km in the solar photosphere, and a spatial resolution of ≃0.″3. The magneotogram noise is $\sigma \simeq 4$ G for single magnetograms, and was computed as the rms of the signal in a sub-field of view (sub-FoV) showing no evident polarization signal (as in, e.g., Gošić et al. 2014) convolved with a 3 × 3 Gaussian kernel. Magnetograms were coaligned, trimmed to the same FoV, which is ≃51 × 53 Mm^2 wide (corresponding to 440 × 455 pixels^2), and filtered out for 5 minute oscillations. Further details can be found in Gošić et al. (2014, 2016).

2.2. Photospheric Electric Field, Current Density, and the Poynting Theorem

In order to compute the plasma horizontal velocity field in the FoV, we applied the Fast Local Correlation Tracking technique (FLCT; Fisher & Welsch 2007, 2008) with a spatial window of ∼1 Mm (10 pixels) to the filtergram time series

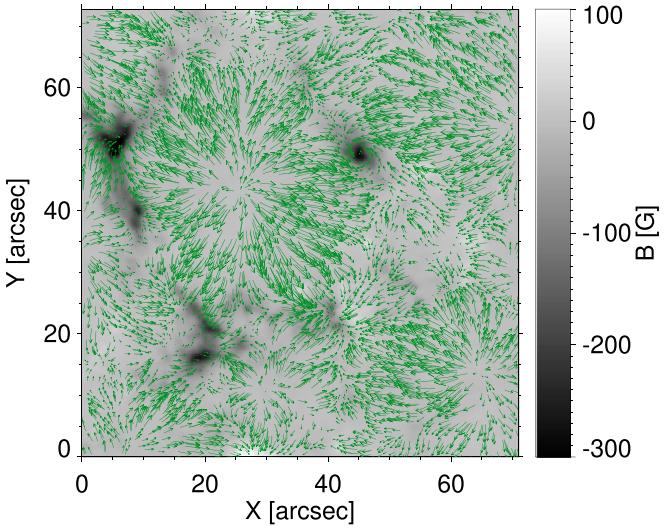

Figure 1. 24 hr averaged magnetogram of the FoV saturated between −300 and 100 G. The boundaries of a supergranular cell are visible as enhancements of negative (black) field strengths. The green arrows represent the horizontal velocity field as computed with the FLCT method (see the text).

simultaneous and cospatial with the magnetogram time series. This method was proved to be very accurate in retrieving the horizontal velocity field when the magnetic field is purely vertical (Schuck 2008). The latter hypothesis will be discussed below and in Section 3. FLCT and its predecessor (the Local Correlation Tracking, LCT) were successfully applied in several works on the same data set, and allowed to obtain results reliable and consistent with previous observations and models (Orozco Suárez et al. 2012; Gošić et al. 2014; Giannattasio et al. 2014b; Requerey et al. 2018; Chian et al. 2019). In particular, Orozco Suárez et al. (2012) showed that the horizontal velocities obtained in the same FoV with the FLCT technique originate radial velocity profiles within the supergranule that are well fitted by the supergranular kinematic model in Simon & Weiss (1989) and Simon et al. (2001). The magnetogram and horizontal velocity time series were then averaged to recover the mean vertical magnetic and horizontal velocity fields over ∼24 hr, which is comparable with the temporal scales characteristic of supergranulation (Rast 2003; Del Moro et al. 2004).

In Figure 1 we show the mean magnetogram averaged over the whole period of observation, T) of the FoV saturated between −300 and 100 G. The boundaries of a supergranular cell are clearly visible as magnetic field enhancements. The green arrows represent the mean horizontal velocity field as computed with the FLCT method (see also Figure 1(a) in Giannattasio et al. 2014b).

In the ideal case of very high magnetic Reynolds numbers (ideal magnetohydrodynamics, MHD, regime) such as those in the solar photosphere (see, e.g., Parker 1963; Weiss 2001; Hirzberger 2002; Cattaneo et al. 2003; Hood & Hughes 2011; Rieutord et al. 2012) the conductivity diverges, and for the Ohm' s law a finite current density, $\boldsymbol{J}$, is possible only if

$$\frac{\boldsymbol{J}}{\sigma} = \boldsymbol{E} + \frac{\boldsymbol{v}}{c} \times \boldsymbol{B} = 0 \Rightarrow \boldsymbol{E} = -\frac{\boldsymbol{v}}{c} \times \boldsymbol{B}, \quad (1)$$

where $\boldsymbol{E}$, $\boldsymbol{B}$, and $\boldsymbol{v}$ are the electric field, the magnetic field, and the plasma velocity, respectively, and we have adopted cgs-Gaussian units. Let us consider the following geometry: the

versor $\hat{\boldsymbol{z}}$ points upward along the direction perpendicular to the photosphere, $\hat{\boldsymbol{y}}$ lays on the photospheric plane and is directed toward the solar north, and $\hat{\boldsymbol{x}}$ completes the orthonormal triad toward the solar east. If we assume that the magnetic field averaged on supergranular timescales T is mainly vertical at photospheric heights (see the discussion in the next section) and in potential configuration (null helicity), namely $\langle \boldsymbol{B} \rangle_T \simeq \langle B_z \rangle_T \hat{\boldsymbol{z}}$ with $\langle B_x \rangle_T \hat{\boldsymbol{x}} = \langle B_y \rangle_T \hat{\boldsymbol{y}} = 0$, we can estimate the average electric field as

$$\langle \boldsymbol{E} \rangle_T = -\frac{1}{c} \langle \boldsymbol{v} \rangle_T \times \langle \boldsymbol{B} \rangle_T. \tag{2}$$

With this prescription the mean electric field reduces to

$$\langle E_x \rangle_T = -\langle v_y \rangle_T \langle B_z \rangle_T / c \;\; \langle E_y \rangle_T = \langle v_x \rangle_T \langle B_z \rangle_T / c \;\; \langle E_z \rangle_T = 0. \tag{3}$$

In using the relations 3 the vertical magnetic field can be evaluated directly from the magnetogram time series and the horizontal velocity field provided by the FLCT technique. In the next section we will discuss the assumption of vertical average magnetic field in the quiet Sun and its evaluation via the magnetogram time series.

The current density that represents the source, at photospheric heights, of the observed magnetic field can be inferred from the Ampere' s law that in cgs-Gaussian units reads

$$\boldsymbol{\nabla} \times \boldsymbol{B} = \frac{4\pi}{c} \boldsymbol{J}, \tag{4}$$

where we have neglected the displacement current. Under the hypothesis of vertical magnetic field when averaging on supergranular timescales Equation (4) gives the solution

$$\langle J_x \rangle_T = \frac{c}{4\pi} \frac{\partial \langle B_z \rangle_T}{\partial y} \quad \langle J_y \rangle_T = -\frac{c}{4\pi} \frac{\partial \langle B_z \rangle_T}{\partial x} \quad \langle J_z \rangle_T = 0. \tag{5}$$

The energy conservation in a plasma volume in the presence of electric and magnetic fields is expressed by the Poynting theorem, which states the relation between the energy density stored into an electromagnetic field, u, the energy flux quantified by the Poynting vector, $\boldsymbol{S}$, and the work done by the fields on a charge distribution. In differential form and for the case $\sigma \rightarrow \infty$ it is written

$$-\frac{\partial u}{\partial t} = \boldsymbol{\nabla} \cdot \boldsymbol{S} + \boldsymbol{J} \cdot \boldsymbol{E}, \tag{6}$$

where $u = B^2/8\pi$ is the (magnetic) field energy per unit volume, $\boldsymbol{S} = \frac{c}{4\pi} \boldsymbol{E} \times \boldsymbol{B}$ is the Poynting vector representing the field energy flux, and $w \equiv \boldsymbol{J} \cdot \boldsymbol{E}$ is the rate of change of plasma mechanical energy per unit volume. Thus, knowing the average photospheric electric and magnetic fields and the current density on supergraular scales, it is possible to estimate the right-hand side of Equation (6) and consequently the average rate of change of field energy per unit volume on the supergranular timescale T, namely $\langle \Delta U \rangle_T$. In particular, we obtain

$$\langle S_x \rangle_T = \frac{c}{4\pi} \langle E_y \rangle_T \langle B_z \rangle_T \;\; \langle S_y \rangle_T = -\frac{c}{4\pi} \langle E_x \rangle_T \langle B_z \rangle_T \;\; \langle S_z \rangle_T = 0, \tag{7}$$

for $\langle \boldsymbol{S} \rangle_T$, which in this case is parallel to $\boldsymbol{v}$, and

$$\langle w \rangle_T = \langle J_x \rangle_T \langle E_x \rangle_T + \langle J_y \rangle_T \langle E_y \rangle_T, \tag{8}$$

for $\langle w \rangle_T$, respectively.

We remark that in the ideal MHD description of plasmas the quantities $\boldsymbol{E}$ and $\boldsymbol{J}$ can be expressed in terms of $\boldsymbol{v}$ and $\boldsymbol{B}$. This means that these pairs of variables can be equivalently used to describe the physical properties of the photospheric plasma. In this work, we computed $\boldsymbol{E}$ and $\boldsymbol{J}$, and for the first time we show their spatial structure in the quiet Sun in an FoV enclosing an entire supergranule. Moreover, the computation of these two quantities provides the terms in the right-hand side (RHS) of Equation (6) together with the evaluation of the left-hand side (LHS) of the same equation, which formally constrains the energy conservation in a plasma volume. Equation (6) will be also used in Section 3 to easily estimate the timescale over which the magnetic energy density changes.

3. Results and Discussion

3.1. Electric Field and Current Density

We computed the photospheric electric field in the FoV under the hypothesis of very high Reynolds numbers and vertical magnetic field over the whole duration $T \simeq 24$ hr of observation by using Equation (3). The computed mean electric field is shown in the upper panel of Figure 2. In that figure, the electric field strength (saturated between $5 \cdot 10^{-5}$ and $3 \cdot 10^{-4}$ statvolt/cm) is represented in grayscale, while its direction is represented with golden arrows. As expected, the photospheric electric field is enhanced (and about one order of magnitude higher) in the boundaries of the supergranular cell, where the magnetic network is located (Giannattasio et al. 2014b), and the horizontal velocity is close to its maximum (Simon & Weiss 1989; Orozco Suárez et al. 2012; Giannattasio et al. 2014b). Due to the mutual directions of $\boldsymbol{v_h}$ and $\boldsymbol{B}$ the electric field in the network regions either crosses the magnetic field concentrations (see, for example, the region in the FoV at $X \in [0''; 10'']$ and $Y \in [35''; 55'']$), or extends radially from them (see, for example, the region of the FoV at $X \in [40''; 50'']$ and $Y \in [45''; 55'']$). As we can see in the horizontal velocity map shown in Figure 1 at the same locations, the former topology is associated with a plasma motion parallel to the supergranular cell boundary and toward increasing Y, while the latter is associated with a counterclockwise whirling motion already detected in previous works (Bonet et al. 2008, 2010; Shelyag et al. 2011; Chian et al. 2019) with a characteristic size of $\lesssim 5''$, corresponding to $\lesssim 3.6$ Mm on the photosphere.

We evaluated the mean current density in the FoV, namely $\langle \boldsymbol{J} \rangle_T$, by computing the components of Equation (5). The results are shown in the lower panel of Figure 2, where the current density strength (saturated between 2,000 and 10,000 statampere/cm^2) is represented in grayscale and its direction with white arrows. As expected, the current density strength is enhanced in correspondence with the magnetic network, and the shape of the current density field is such to encircle the magnetic field concentrations. It is interesting to notice the appearance of current density features that seem to exhibit a hierarchy of vortexes, with the biggest sizes around the strongest magnetic fields and a cascade down to smaller-sized features in the surroundings. This is visible especially in those regions at $Y \lesssim 40''$. In most models of turbulence, vortexes play a fundamental role, and represent a mechanism able to

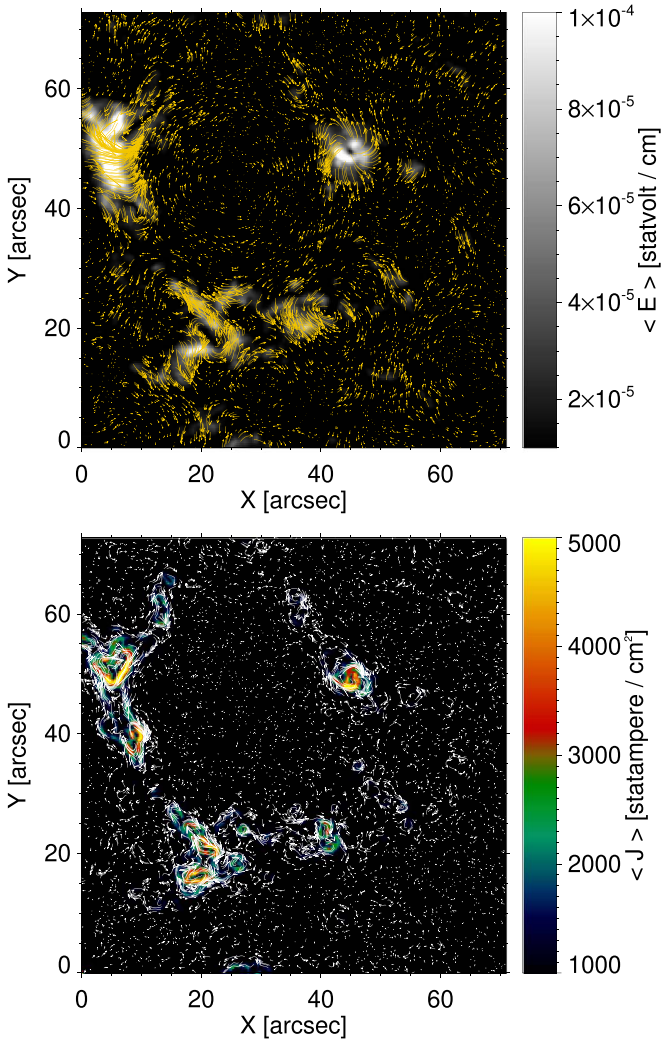

Figure 2. Upper panel: mean electric field computed from Equation (3). The grayscale encodes the field strength, while the golden arrows show the direction of the electric field. Lower panel: mean current density computed from Equation (5). The color encodes the strength, while the white arrows show the direction of the current density.

continuously transfer energy from the largest to the smallest scales, down to the dissipation ones (Frisch 1995). The turbulent nature of the current density features emerging in the FoV used will be investigated in a future work.

We emphasize that the mean electric field and current density were computed under the assumption that the average horizontal component of the magnetic field can be neglected compared to the vertical component, which was estimated by considering the magnetogram time series. This allowed us to use the relations 3 and 5. The question arises: Is this assumption reasonable? In this work we take advantage of an unprecedented 24 hr long magnetogram time series containing a supergranule. Over these spatial and temporal scales, horizontal field components, which typically take place in the internetwork, are expected to average out, making their contribution to the mean magnetic field negligible with respect to that of vertical fields. In fact, it is well known that the magnetic field in the quiet Sun is ubiquitous and quasi-isotropically distributed (Martin 1988; Meunier et al. 1998; Lites 2002; Harvey et al. 2007; López Ariste & Sainz Dalda 2012). The histograms of magnetic field inclination and azimuth are consistent with an isotropic distribution of transverse field associated with the weakest fields and the presence of kilo-Gauss fields that tend to be vertical (Stenflo 1982; Schüssler 1986; Orozco Suárez et al. 2007; Martínez González et al. 2008; Asensio Ramos 2009; Bommier et al. 2009; Ishikawa & Tsuneta 2009; Stenflo 2013). Observational evidence of the isotropic distribution of magnetic field orientations is, for instance, the lack of Hanle rotation when performing inversions of spectropolarimetric data (see, e.g., Bommier et al. 2005; Ishikawa et al. 2008; Ishikawa & Tsuneta 2009, 2010; Bellot Rubio & Orozco Suárez 2019, and references therein). In fact, the improvement of inversion techniques in the last decades made it possible to point out that the azimuth PDFs are nearly flat in the internetwork, indicating a random distribution of orientations of the transverse field component. Thus, on supergranular scales many generations of short-living and arch-shaped bipolar magnetic fields are expected to emerge and evolve in the internetwork with randomly oriented horizontal components; while vertical fields are expected to survive, especially in the network and in the nearby regions, where higher occurrences and longer decorrelation times are observed (Welsch et al. 2012; Giannattasio et al. 2018). Thus, the assumption that the photospheric magnetic field averaged on supergranular scales in the quiet Sun is mainly vertical is reasonable. Under the additional hypothesis that in the observed FoV the magnetic filling factors are $ff = 1$ (Giannattasio et al. 2013), the magnetogram time series used in this work provides a reliable estimation for $\langle \boldsymbol{B} \rangle_T \simeq \langle B_z \rangle_T \hat{\boldsymbol{z}}$.

3.2. The Energy Balance and the Timescales of Energy Exchange

In a recent work, Giannattasio et al. (2018) showed that the decorrelation time of magnetic field in the same FoV, t_D, which is the time after which the autocorrelation function of the pixel-by-pixel magnetogram signal drops to $1/e$, is between $\sim$0.5 and $\sim$4 hr in the supergranular boundaries. This means that the magnetic field on supergranular scales decorrelates well before the decay time τ, and it is not sufficient to consider only the evolution of the magnetic field due to the underneath velocity field in order to explain the much faster decorrelation $t_d < \tau$. We have to consider also the energy that the magnetized plasma exchanges with the surroundings. In fact, both the incoming and outgoing energy flows to/from any plasma volume element may increase/decrease the local energy budget and result in a modification of the magnetic flux content and its consequent decorrelation. Such a local energetic balance is described by the Poynting Theorem (Equation (6)). The simultaneous knowledge of $\langle \boldsymbol{E} \rangle_T$, $\langle \boldsymbol{J} \rangle_T$, and $\langle Bz \rangle_T$ allowed us to estimate the RHS of Equation (6) averaged on supergranular timescales. In that equation, the first term in RHS characterizes the energy flux that can be eventually carried by an electromagnetic field and propagate through a plasma volume element, i.e., the Poynting flux, and $div(\mathbf{S}) > 0$ corresponds to an outflow of energy from the plasma volume element, while $div(\mathbf{S}) < 0$ corresponds to an inflow of energy in the same volume element. The second term of RHS, w, has the dimension of a power per unit volume and provides an estimate of the rate at which the Lorentz force does work on the surrounding plasma causing an increase or decrease of the magnetic energy, u. In particular, a positive variation, $w > 0$, corresponds to a mechanical work done by the fields on the

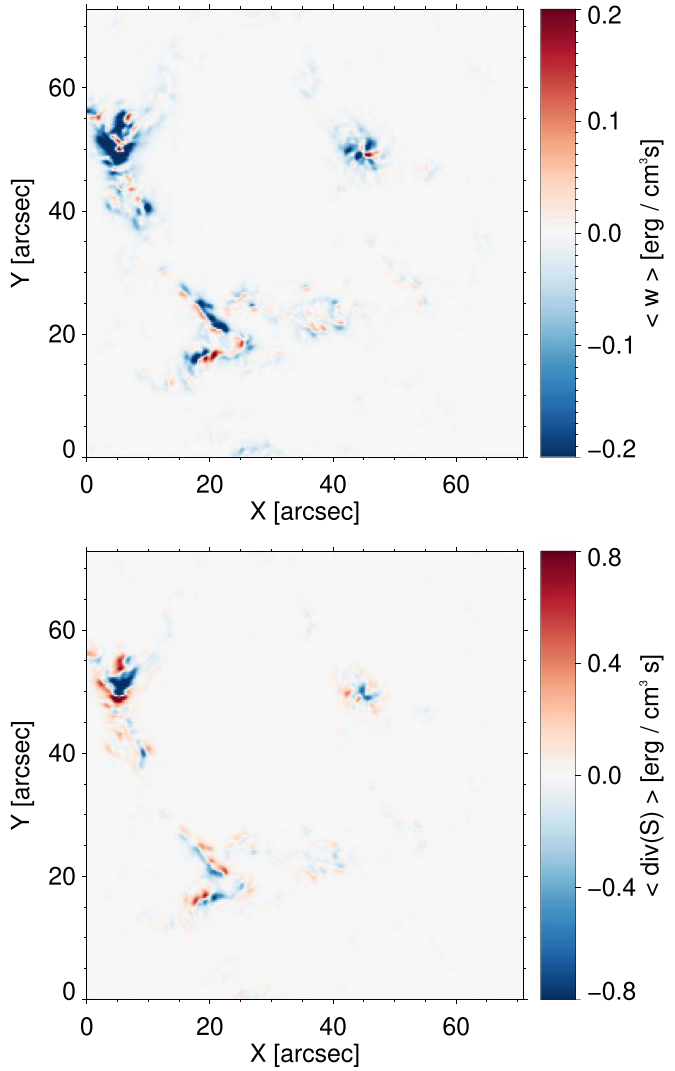

Figure 3. Upper panel: mean energy variation rate, w, due to the Lorentz force. Lower panel: mean divergence of the Poynting vector, i.e., the electromagnetic field energy flux available in the plasma volume element.

surrounding plasma, the more aligned currents and the electric field are, the greater the amount of energy transferred to the surrounding plasma. On the contrary, a negative variation, $w < 0$, corresponds to an increase of internal energy as the Lorentz force does work in the opposite direction, being directed against the electric field from the surrounding plasma to the plasma volume element under consideration. The critical values $div(\mathbf{S}) = 0$ and $w = 0$ correspond, respectively, to a balance between the inflowing/outflowing electromagnetic energy through the volume element and a null exchange of energy with the surrounding plasma. In the upper panel of Figure 3 we show the time-averaged rate of change of mechanical energy per unit volume, w, saturated between -0.2 and $0.2\,\mathrm{erg\,cm^{-3}\,s^{-1}}$ and attributed to the Lorenz force acting on current density via the electric field. The quantity w ranges between -0.92 and $0.27\,\mathrm{erg\,cm^{-3}\,s}$. In correspondence with the supergranular boundaries there is an enhancement of this quantity in absolute value, such that the appearing features are quite symmetrically divided into adjacent subregions with opposite sign (blue/red for negative/positive, respectively). This is consistent with the coexistence of nearby regions where, on average, energy is lost (gained) due to the positive (negative) work done by the Lorenz force per unit volume, the sign being driven by the mutual directions of vectors $\boldsymbol{J}$ and $\boldsymbol{E}$. In these regions the observed transition between positive and negative values of w occurs in the center, where $w = 0$. The only way to satisfy this condition is that the current density and the electric field are mutually orthogonal, as on average neither the former nor the latter are null.

In the lower panel of Figure 3 we show the time-averaged variation of the divergence of the Poynting vector, $div(\mathbf{S})$ that should be associated with an electromagnetic energy flow saturated between -0.8 and $0.8\,\mathrm{erg\,cm^{-3}\,s^{-1}}$. The quantity $div(\mathbf{S})$ ranges between -1.23 and $1.59\,\mathrm{erg\,cm^{-3}\,s}$. Also in this case, in correspondence of the supergranular boundaries there is an enhancement of this quantity in absolute value, which appears to be symmetrically divided into adjacent subregions with opposite sign. This implies the coexistence of nearby regions where, on average, energy is lost (gained) due to the positive (negative) energy flux, the sign being driven by the mutual directions of vectors $\boldsymbol{B}$ and $\boldsymbol{E}$. In these regions the observed transition between positive and negative values of $div(\mathbf{S})$ occurs, again, in the center, where $div(\mathbf{S}) = 0$. The only way to satisfy this condition is that the magnetic and electric fields are parallel, as on average neither the former nor the latter are null. We note that the two RHS terms in Equation (6) are of the same order of magnitude, thus both contribute with the same weight to the estimation of the energy density variation averaged on supergranular scales, namely $\langle \Delta u \rangle_T$.

The timescale, τ^*, associated with the energy variation of a plasma volume element on supergranular scales can be computed by rewriting Equation (6) as follows:

$$\frac{u}{\tau^*} \sim JE + \frac{S}{l}. \tag{9}$$

By assuming $u \simeq B^2/8\pi$ with $B \sim 300$ G as a typical value for the magnetic field in the FoV (Giannattasio et al. 2013), considering the supergranular length scale $l \sim 3 \cdot 10^9$ cm, and once computed the Poynting vector $\mathrm{S} \sim 10^8\ \mathrm{erg\,cm^{-2}\,s}$ we evaluated the timescale of energy exchange

$$\tau^* \sim \frac{B^2 l}{8\pi (JEl + S)} \sim 10^4 s, \tag{10}$$

which corresponds to $\tau^* \sim 2.8$ hr. This timescale is of the same order of magnitude of the magnetic field decorrelation times observed in the same FoV by Giannattasio et al. (2018). This suggests that the energy balance due to the interaction of plasma with both photospheric electric and magnetic fields on supergranular scales plays a crucial role in modifying the magnetic patterns that characterize the photospheric supergranulation. In order to show this, in Figure 4 we show the averaged LHS of Equation (6), $\langle \Delta u \rangle$ on supergranular scales saturated between -1.5 and $1.5\,\mathrm{erg\,cm^{-3}\,s}$. The quantity $\langle \Delta u \rangle$ ranges between -1.76 and $2.08\,\mathrm{erg\,cm^{-3}\,s}$. In that figure, we superposed in green contour plots of the magnetic decorrelation times $t_D > 120$ min computed in Giannattasio et al. (2018). As we can see, the longer t_D times occur mostly where $\langle \Delta u \rangle \geqslant 0$, i.e., where the average energy variation is null or moderately positive. This means that magnetic field decorrelates at longer times mainly where the energy variation is null (in a stationary situation), as we may expect, or the energy slightly increases, as this energy supply is effective in contrasting the field decay

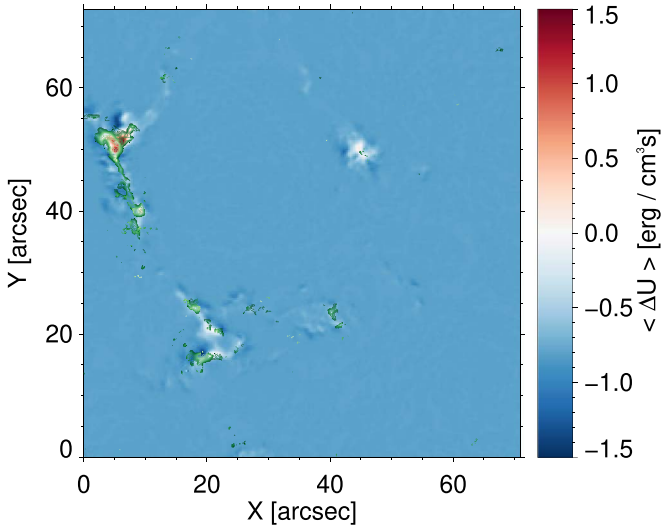

Figure 4. Mean energy variation rate, $\langle \Delta u \rangle$ saturated between -1.5 and 1.5 erg cm^{-3} s. The superposed green lines are contour plots of the magnetic decorrelation times $t_D > 120$ min computed in Giannattasio et al. (2018; see the text).

and the consequent decorrelation. The only exception is represented by the vortex motion observed in the region of the FoV at $X \in [40''; 50'']$ and $Y \in [45''; 55'']$, within which we have basically $\langle \Delta u \rangle \sim 0$, and only a few very small subareas in the center are associated with longer t_D times. As found by Giannattasio et al. (2018) this region is characterized by a very high magnetic field occurrence (near 100%) and $40 \lesssim t_D \lesssim 50$ min, which is probably due to the presence of different and tightly packed magnetic elements moving in a very restricted area. Thus, the lack of magnetic fields with long t_D times in this region with $\langle \Delta u \rangle = 0$ is consistent with the presence of an intense vortex that may act as an attractor constraining the dynamics of the nearby magnetic elements to evolve in a very restricted area and causing these magnetic elements to pile up there. We can interpret these results by depicting the following simple scenario. Turbulent convection produces magnetic fields and drives their motion in the solar photosphere at all scales, from subgranular to supergranular. The coupling between photospheric plasma flows and magnetic fields contributes to the generation of electric fields. The interaction between electric and magnetic fields and plasma currents may alter the local energy content of plasma via, e.g., the Lorentz force and the energy flux flowing through adjacent plasma volumes. For example, a positive work done by the Lorentz force, $w > 0$, accelerates the surrounding plasma in direction of the flows and can, in principle, enhance the currents, while a simultaneous decrease of local energy u occurs. On the contrary, a negative work, $w < 0$, transfers energy to the plasma element causing an increase of u. The same applies to the flux of energy associated with electric and magnetic fields, namely $div(\mathbf{S})$, as an outgoing (incoming) energy from (to) the plasma element corresponds to a decrease (increase) of u. What is important is the balance given by the sum of these two contributions, and it appears clear that there is a correlation between longer magnetic field decorrelation times, t_D, and the regions where $\langle \Delta u \rangle \geqslant 0$. Moreover, when considering the energy balance given by the Poynting theorem, the timescale τ^* on which the magnetic energy density varies is consistent with the decorrelation time of the magnetic field. In particular, τ^* is not long enough to cause, for example, the decay of the supergranule, which must be sustained by both the enhancement of currents and an energy flux coming from the nearby regions, in form, for example, of turbulent transport.

4. Summary and Conclusions

The knowledge of the electric field and current density together with the magnetic field, allows estimation of the energy balance in the photosphere via the Poynting theorem, which links the rate of variation of the energy density in a plasma volume element with the work done by the electric field on the surrounding plasma and the energy flux flowing through the volume element. However, the computation of local electric field at any time requires the knowledge, for example, of the vector magnetic field, which can be obtained only via the inversion of spectropolarimetric (SP) full-Stokes data. On the other hand, it is not possible to acquire long SP data targeted at large FoVs with fast cadence and high spectropolarimetric sensitivity, since this experimental setup has the result of reducing the number of spectral points sampled, which affects the goodness of results, and vice versa. Despite this, we can still obtain a reasonable approximation for the electric field averaged on supergranular scales by using only magnetogram time series instead of full-Stokes data. Our findings may be itemized as follows:

1. For the first time we provided average photospheric electric field and current density in the quiet Sun on supergranular scales by using a ∼24 hr long magnetogram time series enclosing an entire supergranule.
2. By applying the Poynting theorem we computed the average rate of change of field energy per unit volume on supergranular scales, $\langle \Delta u \rangle$, and found that the timescale associated with the energy variation is consistent with the magnetic field decorrelation times, t_D, in the same FoV retrieved in Giannattasio et al. (2018).
3. The longer t_D times are cospatial with the regions where $\langle \Delta u \rangle \geqslant 0$, indicating that the energy supply effectively balances the magnetic field and energy decay.

We regard that this study could represent a turning point for the exploitation of long magnetogram time series to investigate more comprehensively the energy balance at large and long scales. Due to the huge amount of magnetic flux emerging in the quiet Sun, this energy greatly contributes to sustain the upper atmospheric layers.

This work is supported by the Italian MIUR-PRIN grant 2017APKP7T on *Circumterrestrial Environment: Impact of Sun-Earth Interaction*. F.G. is grateful to M. Gošić and L. Bellot Rubio for providing the data analyzed here. This paper is based on data acquired in the framework of the Hinode Operation Plan 151 entitled "Flux replacement in the network and internetwork". Hinode is a Japanese mission developed and launched by ISAS/JAXA, collaborating with NAOJ as a domestic partner, as well as NASA and STFC (UK) as international partners. Scientific operation of the Hinode mission is conducted by the Hinode science team organized at ISAS/JAXA. This team mainly consists of scientists from

institutes in the partner countries. Support for the post-launch operation is provided by JAXA and NAOJ (Japan), STFC (U.K.), NASA, ESA, and NSC (Norway).

ORCID iDs

Fabio Giannattasio https://orcid.org/0000-0002-9691-8910
Giuseppe Consolini https://orcid.org/0000-0002-3403-647X
Francesco Berrilli https://orcid.org/0000-0002-2276-3733
Dario Del Moro https://orcid.org/0000-0003-2500-5054

References

Abramenko, V. I. 2017, MNRAS, 471, 3871
Asensio Ramos, A. 2009, ApJ, 701, 1032
Bellot Rubio, L., & Orozco Suárez, D. 2019, LRSP, 16, 1
Bommier, V., Derouich, M., Landi Degl'Innocenti, E., Molodij, G., & Sahal-Bréchot, S. 2005, A&A, 432, 295
Bommier, V., Martínez González, M., Bianda, M., et al. 2009, A&A, 506, 1415
Bonet, J. A., Márquez, I., Sánchez Almeida, J., et al. 2010, ApJL, 723, L139
Bonet, J. A., Márquez, I., Sánchez Almeida, J., Cabello, I., & Domingo, V. 2008, ApJL, 687, L131
Cattaneo, F., Emonet, T., & Weiss, N. 2003, ApJ, 588, 1183
Chae, J. 1999, in ASP Conf. Ser. 183, High Resolution Solar Physics: Theory, Observations, and Techniques, ed. T. R. Rimmele, K. S. Balasubramaniam, & R. R. Radick (San Francisco, CA: ASP), 375
Chae, J., & Sakurai, T. 2008, ApJ, 689, 593
Chian, A. C. L., Silva, S. S. A., Rempel, E. L., et al. 2019, MNRAS, 488, 3076
Davis, W. D. 1977, SoPh, 54, 139
Del Moro, D., Berrilli, F., Duvall, T. L. J., & Kosovichev, A. G. 2004, SoPh, 221, 23
Démoulin, P., & Berger, M. A. 2003, SoPh, 215, 203
Fisher, G. H., & Welsch, B. 2007, AAS Meeting, 210, 92.11
Fisher, G. H., & Welsch, B. T. 2008, in ASP Conf. Ser. 383, Subsurface and Atmospheric Influences on Solar Activity, ed. R. Howe et al. (San Francisco, CA: ASP), 373
Fisher, G. H., Welsch, B. T., Abbett, W. P., & Bercik, D. J. 2010, ApJ, 715, 242
Frisch, U. 1995, Turbulence: The Legacy of A. N. Kolmogorov (Cambridge: Cambridge Univ. Press)
Giannattasio, F., Berrilli, F., Biferale, L., et al. 2014a, A&A, 569, A121
Giannattasio, F., Berrilli, F., Consolini, G., et al. 2018, A&A, 611, A56
Giannattasio, F., Consolini, G., Berrilli, F., & Del Moro, D. 2019, ApJ, 878, 33
Giannattasio, F., Del Moro, D., Berrilli, F., et al. 2013, ApJL, 770, L36
Giannattasio, F., Stangalini, M., Berrilli, F., Del Moro, D., & Bellot Rubio, L. 2014b, ApJ, 788, 137
Gošić, M., Bellot Rubio, L. R., del Toro Iniesta, J. C., Orozco Suárez, D., & Katsukawa, Y. 2016, ApJ, 820, 35
Gošić, M., Bellot Rubio, L. R., Orozco Suárez, D., Katsukawa, Y., & del Toro Iniesta, J. C. 2014, ApJ, 797, 49
Gošić, M., de la Cruz Rodríguez, J., De Pontieu, B., et al. 2018, ApJ, 857, 48
Hahn, M., & Savin, D. W. 2014, ApJ, 795, 111
Harvey, J. W., Branston, D., Henney, C. J., Keller, C. U. & SOLIS and GONG Teams. 2007, ApJL, 659, L177
Hirzberger, J. 2002, A&A, 392, 1105
Hood, A. W., & Hughes, D. W. 2011, PEPI, 187, 78
Ishikawa, R., & Tsuneta, S. 2009, A&A, 495, 607
Ishikawa, R., & Tsuneta, S. 2010, ApJL, 718, L171
Ishikawa, R., Tsuneta, S., Ichimoto, K., et al. 2008, A&A, 481, L25
Jefferies, S. M., Fleck, B., Murphy, N., & Berrilli, F. 2019, ApJL, 884, L8
Jordan, C., Bartoe, J. D. F., & Brueckner, G. E. 1980, ApJ, 240, 702
Kazachenko, M. D., Fisher, G. H., & Welsch, B. T. 2014, ApJ, 795, 17
Kazachenko, M. D., Fisher, G. H., Welsch, B. T., Liu, Y., & Sun, X. 2015, ApJ, 811, 16
Kosugi, T., Matsuzaki, K., Sakao, T., et al. 2007, SoPh, 243, 3
Kusano, K., Maeshiro, T., Yokoyama, T., & Sakurai, T. 2002, ApJ, 577, 501
Lites, B. W. 2002, ApJ, 573, 431
López Ariste, A., & Sainz Dalda, A. 2012, A&A, 540, A66
Martin, S. F. 1988, SoPh, 117, 243
Martínez González, M. J., Asensio Ramos, A., López Ariste, A., & Manso Sainz, R. 2008, A&A, 479, 229
Meunier, N., Solanki, S. K., & Livingston, W. C. 1998, A&A, 331, 771
Moran, T., & Foukal, P. 1991, SoPh, 135, 179
Orozco Suárez, D., Bellot Rubio, L. R., del Toro Iniesta, J. C., et al. 2007, ApJL, 670, L61
Orozco Suárez, D., Katsukawa, Y., & Bellot Rubio, L. R. 2012, ApJL, 758, L38
Parker, E. N. 1963, ApJ, 138, 552
Rajaguru, S. P., Sangeetha, C. R., & Tripathi, D. 2019, ApJ, 871, 155
Rast, M. P. 2003, ApJ, 597, 1200
Requerey, I. S., Cobo, B. R., Gošić, M., & Bellot Rubio, L. R. 2018, A&A, 610, A84
Rieutord, M., Rincon, F., & Roudier, T. 2012, in EAS Publ. Ser. 55, Understanding Solar Activity: Advances and Challenges, ed. M. Faurobert, C. Fang, & T. Corbard (Les Ulis: EDP Sciences), 5
Rouppe van der Voort, L. H. M., Rutten, R. J., & Vissers, G. J. M. 2016, A&A, 592, A100
Schuck, P. W. 2006, ApJ, 646, 1358
Schuck, P. W. 2008, ApJ, 683, 1134
Schüssler, M. 1986, in Small Scale Magnetic Flux Concentrations in the Solar Photosphere, ed. W. Deinzer, M. Knölker, & H. H. Voigt (Göttingen: Vandenhoeck & Ruprecht), 103
Shelyag, S., Keys, P., Mathioudakis, M., & Keenan, F. P. 2011, A&A, 526, A5
Simon, G. W., Title, A. M., & Weiss, N. O. 2001, ApJ, 561, 427
Simon, G. W., & Weiss, N. O. 1989, ApJ, 345, 1060
Stangalini, M., Giannattasio, F., & Jafarzadeh, S. 2015, A&A, 577, A17
Stenflo, J. O. 1982, SoPh, 80, 209
Stenflo, J. O. 2013, A&ARv, 21, 66
Trujillo Bueno, J., Shchukina, N., & Asensio Ramos, A. 2004, Natur, 430, 326
Tsuneta, S., Ichimoto, K., Katsukawa, Y., et al. 2008, SoPh, 249, 167
Viticchié, B., Del Moro, D., & Berrilli, F. 2006, ApJ, 652, 1734
Weiss, N. 2001, A&G, 42, 3.10
Welsch, B. T., Fisher, G. H., Abbett, W. P., & Regnier, S. 2004, ApJ, 610, 1148
Welsch, B. T., Kusano, K., Yamamoto, T. T., & Muglach, K. 2012, ApJ, 747, 130
Wien, W. 1916, AnP, 354, 842